Ex Vivo Human Placenta Perfusion, Metabolic and Functional Imaging for Obstetric Research—A Feasibility Study

Katrine Elbæk Madsen[1,2], Christian Østergaard Mariager[1], Christina S. Duvald[2], Esben Søvsø Szocska Hansen[1], Lotte Bonde Bertelsen[1], Michael Pedersen[2], Lars Henning Pedersen[3], Niels Uldbjerg[3], and Christoffer Laustsen[1]

[1]Department of Clinical Medicine, MR-Research Centre, Aarhus University, Aarhus, Denmark; [2]Department of Clinical Medicine, Comparative Medicine Laboratory, Aarhus University, Aarhus, Denmark; and [3]Department of Gynaecology and Obstetrics, Aarhus University Hospital and Department of Clinical Medicine, Aarhus University, Aarhus, Denmark

Corresponding Author:
Christoffer Laustsen, PhD
Arhus University Hospital, Palle Juul Jensens Boulevard 99, Arhus, Denmark 8200;
E-mail: cl@clin.au.dk

Key Words: Placenta, metabolism, hyperpolarization, 13C, pyruvate, MRI
Abbreviations: glucose transporters (GLUT), monocarboxylic transporters (MCT), magnetic resonance imaging (MRI), repetition time (TR), lactate dehydrogenase (LDH)

ABSTRACT

Placenta metabolism is closely linked to pregnancy outcome, and few modalities are currently available for studying the human placenta. Here, we aimed to investigate a novel ex vivo human placenta perfusion system for metabolic imaging using hyperpolarized [1-^{13}C]pyruvate. The metabolic effects of 3 different human placentas were investigated using functional and metabolic magnetic resonance imaging. The placenta glucose metabolism and hemodynamics were characterized with hyperpolarized [1-^{13}C]pyruvate magnetic resonance imaging and by dynamic contrast-enhanced (DCE) imaging. Hyperpolarized [1-^{13}C]pyruvate showed a decrease in the ^{13}C-lactate/^{13}C-pyruvate ratio from the highest to the lowest metabolic active placenta. The metabolic profile was complemented by a more homogenous distributed hemodynamic response, with a longer mean transit time and higher blood volume. This study shows different placenta metabolic and hemodynamic features associated with the placenta functional status using hyperpolarized magnetic resonance ex vivo. This study supports further studies using ex vivo metabolic imaging of the placenta alterations associated with pregnancy complications.

INTRODUCTION

The placenta is an endocrine organ with a high metabolic demand. It produces several hormones that are essential for a normal pregnancy outcome (1). Furthermore, several pregnancy complications, such as fetal growth restriction, preeclampsia, and gestational diabetes, are associated with abnormal placental endocrine function (2–6). The processes are complex, illustrated by a maternofetal glucose transfer that depends on the density of glucose transporters (GLUT), primarily in the rate-limiting basal membrane of the placenta (7). The expression of GLUT1 (8, 9), GLUT4, and GLUT9 (9) is increased in diabetic pregnancies and this expression is also associated with fetal birth weight (9). In vitro experiments have however identified an inverse relationship between the expression of glucose and GLUT1 (8), and, consequently, hyperglycemia per se does not seem to explain the in vivo observations mentioned earlier. Increasing evidence supports lactate as an important energy source in fetoplacental energy production (10, 11). Interestingly, a higher concentration of lactate is found in fetal circulation than in maternal circulation (11). This inverse concentration gradient compared with glucose is driven by 2 monocarboxylic transporters—MCT1 and MCT4 (12) (Figure 1A). Overall, we know little about the physiology and involvement in pathophysiology of these pathways in the placenta.

The MCTs have previously been shown to be important mediators of in vivo lactate production seen in hyperpolarized ^{13}C magnetic resonance spectroscopy studies of both preclinical models and in humans (14), which in turn have been shown to be directly linked to pathophysiological conditions such as diabetes, where an upregulated lactate production has been observed in the heart, liver, and kidneys (15–17).

Ex vivo angiography can elucidate vascular structures 3-dimensionally with simultaneous estimation of intravascular volume of the placenta (13). To yield direct metabolic information on glucose metabolism in the placenta, we here propose to add metabolic imaging using hyperpolarized ^{13}C spectroscopy to the placental angiography.

Hyperpolarized [1-^{13}C]-pyruvate magnetic resonance imaging (MRI) allows imaging of the glycolytic pathway,

ISSN 2379-1381 https://doi.org/10.18383/j.tom.2019.00016

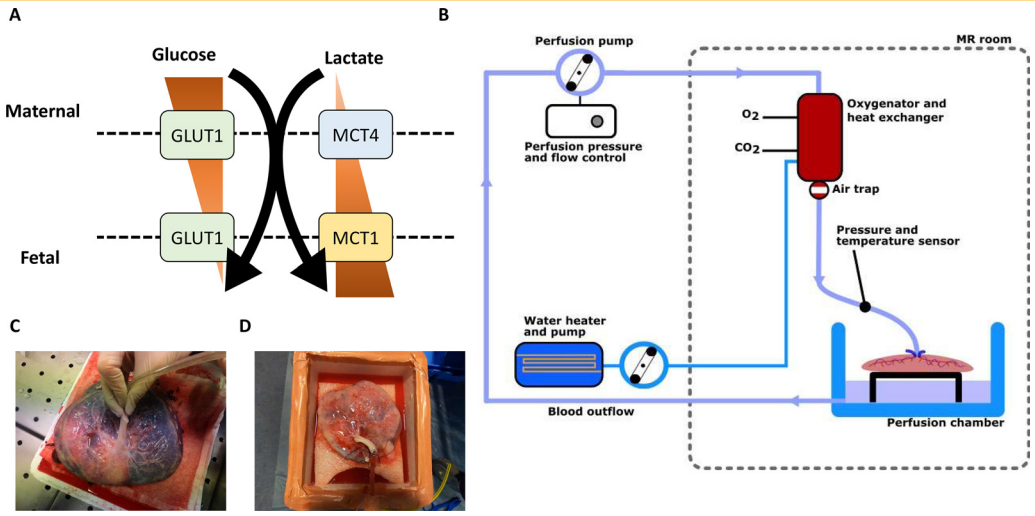

Figure 1. Schematic of the current knowledge of glucose and lactate transport from the maternal to the fetal side (A). Perfusion setup (B). Flushing the placental vascular bed with an appropriate extension line (C). The attaching of the placenta to the perfusion loop (D).

resulting in maps of pyruvate and its derivatives: lactate, alanine, and bicarbonate. This method has recently been used to noninvasively examine the fetoplacental transport and utilization of these substances in chinchillas (18), followed by a hyperpolarized [1-^{13}C]-pyruvate MRI study in placentas of naïve and diseased pregnant rats (19). We hypothesize that the pyruvate metabolism can be imaged in the human placenta with the same technique. In this feasibility study, we aimed to introduce hyperpolarized ^{13}C-labeled MRI as a novel method for the examination of glucose metabolism in human placentas perfused ex vivo.

METHODS

Placental Preparation

We included 3 normal placentas from elective caesarean sections conducted at term of pregnancy with no suspicion of placenta dysfunction, the placentas were anonymized, and no information was obtained on the mother, about the pregnancy, or the child. Immediately after delivery, the 3 placentas were placed on a cloth on top of ice and brought to the MRI research laboratory. Within 30 minutes, the umbilical cord was cut at about 5 cm from the placenta and the 2 umbilical arteries were cannulated (Figure 1C), flushed with heparinized saline (5°C, 5000 UI/L), and connected to the perfusion system.

Ex Vivo Placenta Perfusion System

The in-house-developed perfusion system as illustrated in Figure 1B was feasible for a single cotyledon (20, 21) and the whole placenta (22) perfusion. The system comprised a centrifugal pump (BioMedicus Medtronic Bio-Console 540; Medtronic, Minneapolis, MN), giving 1–70 mL/min of Krebs–Henseleit buffer, heated to 37°C, and oxygenated with carbogen (95% O_2/5% CO_2) using a Medos Hilite 1000 neonatal oxygenator (Xenios, Heilbronn, Germany).

The 3 placentas were immersed in a Styrofoam box with the Krebs–Henseleit buffer solution, and 2 artery adaptors were connected to extension line as illustrated in Figure 1D. The perfusate entered the placental circulation through the arteries and left it through the umbilical vein, into the box from where it re-entered the loop by mean of suction.

Magnetic Resonance Imaging

Imaging was performed on a 3 T Signa HDx MRI scanner (GE Healthcare, Milwaukee, WI) equipped with a 2 element ^{1}H array coil (GE Healthcare) and Clamshell ^{13}C transmit coil (Rapid Biomedical GmbH, Rimpar, Germany). The perfusion chamber with the placenta was placed in the scanner isocenter such that the middle of the organ coincided with the radiofrequency center of both coils. The placental anatomy was found using a T2-weighted PROPELLER MRI sequence, using the following parameters: T2-PROPELLER: repetition time (TR) = 7.4 seconds, echo time = 92 milliseconds, flip angle = 142°, field of view = 260 × 260 mm^2, matrix = 256 × 256, long-axis slices = 10, and slice thickness = 4 mm, averages = 4.

The placental pyruvate metabolism was visualized using hyperpolarized [1-^{13}C]pyruvate magnetic resonance spectroscopy within 1–2 hours after delivery. ^{1}H anatomical MRI was performed to allow placement of a 10° slice-selective ^{13}C free inductive decay spectroscopy time series with a 1-second TR and 180 interleaves, spectral width 5000 Hz and 2048 number of points, covering the full placenta. The hyperpolarized ^{13}C experiments were performed subsequent to a 9-mL injection of 80mM hyperpolarized [1-^{13}C] pyruvate into the perfusion system over a period of 5 seconds. The ^{13}C free inductive decay spectroscopy was analyzed using an in-house general linear model approach in Matlab 2018b (The MathWorks Inc., Natick, Massachusetts). The [1-^{13}C]lactate AUC signal was normalized by the [1-^{13}C]pyruvate AUC signal. MRI acquisition was initiated just before the

Table 1. Primer Sequences

Gene	Forward Primer Sequence	Reverse Primer Sequence
RPL22	5′- GGAGCAAGAGCAAGATCACC-3′	5′-TGTTAGCAACTACGCGCAAC-3′
LDHA	5′-GAAAGCTGTCATGGGCTGAT-3′	5′-GTGGACATTTTCCCACTGCT-3′
MCT1	5′-TGGATGGAGAGGAAGCTTTCTAAT-3′	5′-CACACCAGATTTTCCAGCTTTC-3′
MCT4	5′-CACGGCATCGTCACCAACT-3′	5′-ACAGCCTGGATAGCAACGTACAT-3′

[1-^{13}C]-pyruvate injection and continued for 2–3 minutes. Lastly, perfusion was assessed using dynamic contrast-enhanced MRI following an injection of 0.3-mL Dotarem, using a 3D fast gradient echo DISCO sequence having the following parameters: TR= 1.9 seconds, echo time = 1.8 milliseconds, flip angle = 30°, field of view = 300 × 300 × 300 mm^3, and matrix = 256 × 256.

qPCR and Activity Assay

Following the magnetic resonance examination, tissue samples (N = 3) were taken from the placentas; the samples were taken at random from the full placenta, with no specific action initiated to ensure visually similar tissue. This approach was used to get a more representative image of the potential heterogeneity. Placental tissues were used for analyzing the lactate dehydrogenase (LDH) activity as well as the mRNA expression of LDH and MCT1 and MCT4. To ensure activity measurement, tissues were instantly frozen in liquid nitrogen and stored at −80°C.

LDH Activity Assay

The assay was performed according to the manufacturer's instructions with few alterations (Sigma-Aldrich, Copenhagen, Denmark). In brief, the placenta tissue was homogenized in an assay buffer. The homogenate was centrifuged, and the assay was performed on the resultant supernatant. Analysis was performed in 384-well plates in a microplate reader (SYNERGY H1; Biotek, Aarhus, Denmark). Absorbance reading was performed at the highest peak in the absorbance spectrum (462 nm). Activity measurements were normalized to protein amount in the LDH sample solution. Protein quantification was measured by using a Qubit 3.0 flourometer (Fisher Scientific, Wilmington, DE).

Quantitative Real-Time PCR

Placental tissue was homogenized, and total RNA was isolated using a Nucleospin RNA II kit (Stratagene; AH Diagnostics, Aarhus, Denmark) following the manufacturer's instructions.

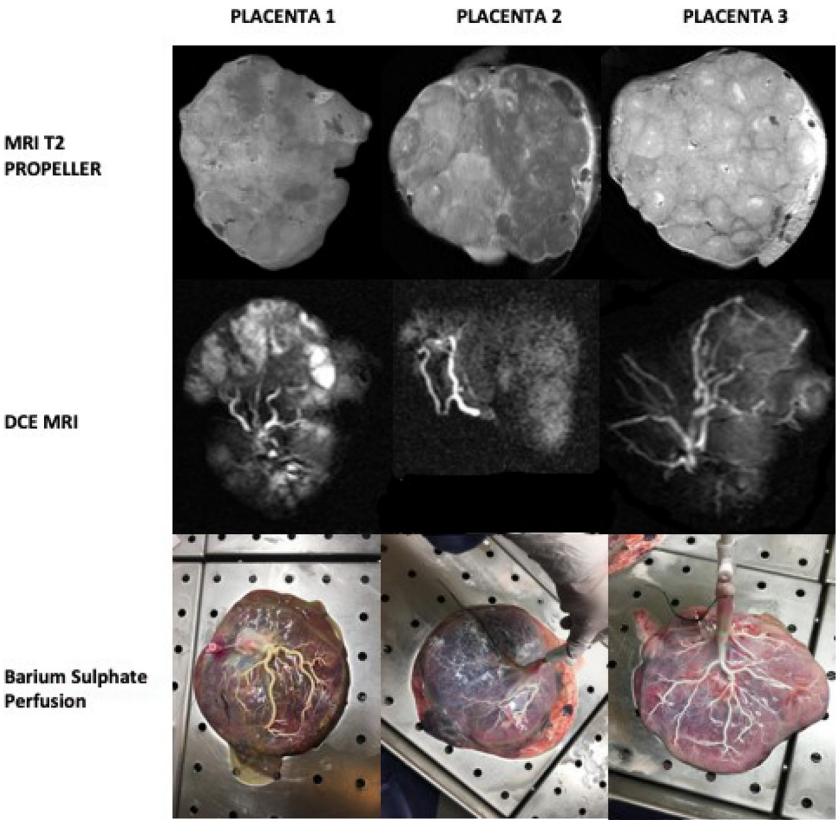

Figure 2. Top row: T2-weighted magnetic resonance imaging (MRI) showing the differences in contrast between the 3 placentas. Middle row: magnetic resnoance angiography acqusition showing distribution of the contrast agent. Bottom row: barium sulphate perfusion images of the 3 placentas.

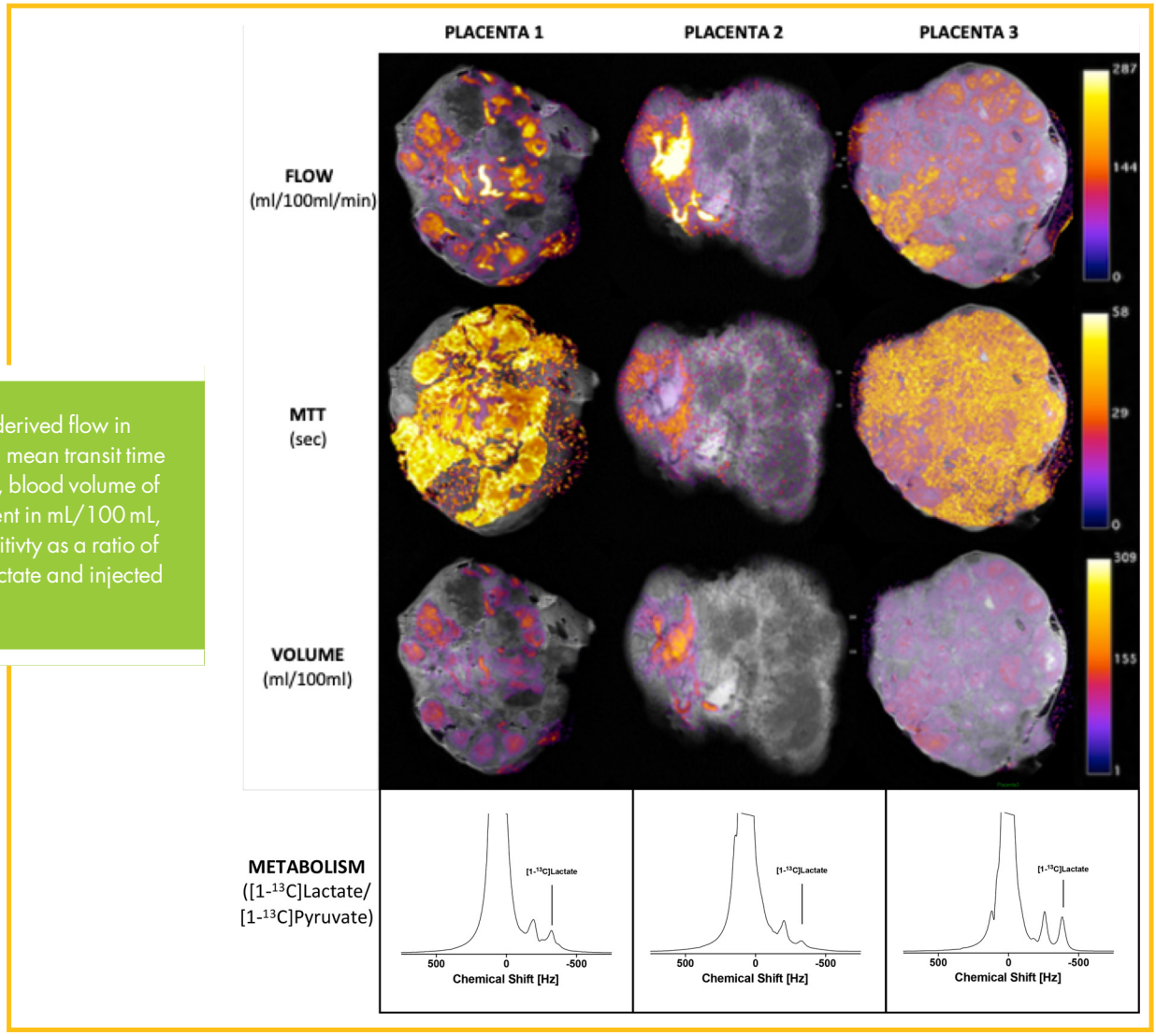

Figure 3. MRI-derived flow in mL/100 mL/min, mean transit time (MTT) in seconds, blood volume of the perfusion agent in mL/100 mL, and glycolytic acitivty as a ratio of produced ^{13}C-lactate and injected ^{13}C-pyruvate.

RNA concentration was confirmed by the use of a Qubit 3.0 flourometer. CDNA synthesis was performed with RevertAid First Strand cDNA synthesis kit (Thermo Scientific). qPCR was performed using SYBR Green qPCR Master Mix according to manufacturer's instructions (Stratagene). In brief, 100 ng of cDNA was used as template for PCR amplification, and the specificity of products was confirmed by using the melting curve analysis. Real-time qPCR was performed on an Agilent Ariamx real-time system (Agilent Technologies, Santa Clara, CA). The primers used for qPCR are shown in Table 1.

RESULTS

Contrast-enhanced and noncontrast-enhanced MRI, as well as barium sulfate perfusion, revealed individual cotyledons in all 3 placentas, however, with a heterogeneous appearance (Figure 2), indicating low perfusion in some parts of the placenta and high perfusion in other parts. In placenta 2, this might be associated to different perfusion of the 2 parts supplied each of the 2 umbilical arteries. Similar trends were observed with the placenta blood perfusion, mean transit time and vascular volume (volume of distribution; Figure 3, Table 2). With respect to these hemodynamic changes, the metabolic [1-^{13}C]-pyruvate profiles differed as expressed by the lactate-to-pyruvate ratios (placenta 2 < placenta 1 < placenta 3) as shown in Table 2. To determine the origin of the observed metabolic changes, gene expression and LDH activity assays were performed on randomly sampled biopsies from the 3 different placentas. A tendency toward a lower LDH activity in placenta 2 than in placenta 1 and placenta 3 was observed. Similarly, MCT1 expression was not reduced in placenta 2 compared with that in the placentas 1 and 3. MCT4 and LDH expressions was not different (Table 2).

DISCUSSION

The main finding in this study was the ability to distinguish hemodynamic and metabolic features of the human placenta ex vivo, using hyperpolarized [1-^{13}C]-pyruvate MRI as a feasible approach. These findings indicate that even with an almost-identical overall hemodynamic response, local heterogeneous variations, imposed during the preparation procedure, result in large variations in the placental metabolic profile. The metabolic

Table 2. Hemodynamic and Metabolic Placenta Features

	Mean Perfusion	MTT	VoD	*Lactate AUC / Pyruvate AUC*	LDH Activity	LDH mRNA	MCT1	MCT4
	mL/100 mL/Min	s	mL/100 mL	Ratio	U/μg	LDH/RPL22 Ratio	MCT1/RPL22 Ratio	MCT4/RPL22 Ratio
Placenta 1	40.8	31.2	17.8	0.034	15e3 ± 11e3	0.19 ± 0.09	1.6 ± 1.4	0.02 ± 0.01
Placenta 2	41.1	14.6	9.5	0.018	2e3 ± 1e3	0.06 ± 0.03	1.5 ± 0.4	0.01 ± 0.01
Placenta 3	43.8	32.6	23.0	0.052	14e3 ± 11e3	0.12 ± 0.11	2.2 ± 0.6	0.01 ± 0.02

Abbreviations: MTT, mean perfusion, mean transit time; VoD, volume of distribution; AUC, lactate-to-pyruvate area under curve ratio. *Ex Vivo Biopsy Assays*. Lactate dehydrogenase (LDH) Activity and LDH mRNA Expression. Monocarboxylate transporter (MCT) 1 and MCT4 mRNA Expression.

profile was found to be very closely related to the mean transit time and the blood volume (volume of distribution), which as such indicate that the metabolic profile is directly related to the delivery of nutrients and pyruvate to the tissue. The heterogeneous metabolic patterns were confirmed by random sampling biopsies, supporting the use of hyperpolarized MRI as a novel method to provide additional information on placenta function. With a seemingly higher LDH activity in placenta 1 and placenta 3 than in placenta 2, this study also suggests of a relationship between vascular volume and metabolic conversion of pyruvate. Taken together, these support further investigations by means of this new tool to improve our understanding about the placenta and the alterations in function associated with pregnancy complications, as well as potential therapeutic effects. A potential limitation is the low perfusion rate used in the placentas. Previous reports have used higher perfusions rates (250 mL/min) for whole-placenta perfusion (22), which could in part result in higher metabolic conversion. However, this can be contradicted by the fact that maternal and fetal sides have very distinct differences in blood and, thus, could impose reactions and as such high perfusion rates is not necessarily a good option in all cases. The variation seen in this study is likely originating from the preparation procedures, insufficient perfusion, and/or variation in the time from C-section to perfusion and perfusion time, rather than reflecting an actual difference in the placenta perfusion and metabolism. This is supported by the fact that the placentas were from uncomplicated pregnancies and C-sections. These limitations need to be further explored in future studies. Furthermore an improved ^{13}C imaging strategy to resolve the local metabolic heterogeneity indicated with the ^{1}H imaging is essential. The method needs to improve the sensitivity, thereby allowing the oxidative metabolism estimation via pyruvate dehydrogenase (PDH) flux, as seen by the production of $^{13}CO_2$ and $H^{13}CO_3^-$ and amino acid synthesis via alanine transaminase (ALT).

Hyperpolarized [1-^{13}C]-pyruvate MRI is a promising new ex vivo method that can easily be implemented in both clinical and preclinical scanners and do not require extensive approval and pharmacy preparations. As such, hyperpolarized ex vivo placenta [1-^{13}C]-pyruvate MRI represents an alternative route to many of the hyperpolarized human studies that are currently ongoing (14), both as a stand-alone method and in combination with in vivo [1-^{13}C]pyruvate imaging of the placenta (18, 19, 23). Further studies are needed to validate the methods' repeatability and reproducibility and its ability to evaluate hemodynamic and metabolic alterations in pregnancy complications. The combination of [1-^{13}C]pyruvate or [1-^{13}C]lactate with ^{18}FDG positron emission tomography can potentially enable even more insights into the underlying physiology and the pathophysiology in the fetoplacental transport (GLUT and MCTs) and utilization of glucose and lactate.

REFERENCES

1. Bauer MK, Harding JE, Bassett NS, Breier BH, Oliver MH, Gallaher BH, Evans PC, Woodall SM, Gluckman PD. Fetal growth and placental function. Mol Cell Endocrinol. 1998;140:115–120.
2. Magnusson AL, Powell T, Wennergren M, Jansson T. Glucose metabolism in the human preterm and term placenta of IUGR fetuses. Placenta. 2004;25:337–346.
3. Challis DE, Pfarrer CD, Ritchie JW, Koren G, Adamson SL. Glucose metabolism is elevated and vascular resistance and maternofetal transfer is normal in perfused placental cotyledons from severely growth-restricted fetuses. Pediatr Res. 2000;47:309–315.
4. Bahr BL, Price MD, Merrill D, Mejia C, Call L, Bearss D, Arroyo J. Different expression of placental pyruvate kinase in normal, preeclamptic and intrauterine growth restriction pregnancies. Placenta. 2014;35:883–890.
5. Cirkel U, Burkart W, Stahler E, Buchholz R. Effects of alloxan-induced diabetes mellitus on the metabolism of the rat placenta. Arch Gynecol. 1986;237:155–163.
6. Martin RJ, Makula A, Kasser TR. Placental metabolism and enzyme activities in diabetic pigs. Proc Soc Exp Biol Med. 1980;165:39–43.
7. Vardhana PA, Illsley NP. Transepithelial glucose transport and metabolism in BeWo choriocarcinoma cells. Placenta. 2002;23:653–660.
8. Baumann MU, Deborde S, Illsley NP. Placental glucose transfer and fetal growth. Endocrine. 2002;19:13–22.
9. Stanirowski PJ, Szukiewicz D, Pyzlak M, Abdalla N, Sawicki W, Cendrowski K. Analysis of correlations between the placental expression of glucose transporters GLUT-1, GLUT-4 and GLUT-9 and selected maternal and fetal parameters in pregnancies complicated by diabetes mellitus. J Matern Fetal Neonatal Med. 2019;32:650–659.
10. Burd LI, Jones MD, Simmons MA, Makowski EL, Meschia G, Battaglia FC. Placental production and foetal utilisation of lactate and pyruvate. Nature. 1975;254:710–711.
11. Suidan JS, Antoine C, Silverman F, Lustig ID, Wasserman JF, Young BK. Human maternal-fetal lactate relationships. J Perinat Med. 1984;12:211–217.
12. Nagai A, Takebe K, Nio-Kobayashi J, Takahashi-Iwanaga H, Iwanaga T. Cellular expression of the monocarboxylate transporter (MCT) family in the placenta of mice. Placenta. 2010;31:126–133.
13. Rasmussen AS, Lauridsen H, Laustsen C, Jensen BG, Pedersen SF, Uhrenholt L, Boel LWT, Uldbjerg N, Wang T, Pedersen M. High-resolution ex vivo magnetic resonance angiography: a feasibility study on biological and medical tissues. BMC Physiol. 2010;10:3–3.

14. Kurhanewicz J, Vigneron DB, Ardenkjaer-Larsen JH, Bankson JA, Brindle K, Cunningham CH, Gallagher FA, Keshari KR, Kjaer A, Laustsen C, Mankoff DA, Merritt ME, Nelson SJ, Pauly JM, Lee P, Ronen S, Tyler DJ, Rajan SS, Spielman DM, Wald L, Zhang X, Malloy CR, Rizi R. Hyperpolarized (13)C MRI: path to clinical translation in oncology. Neoplasia. 2019; 21:1–16.
15. Lewis AJM, Miller JJJ, McCallum C, Rider OJ, Neubauer S, Heather LC, Tyler DJ. Assessment of metformin-induced changes in cardiac and hepatic redox state using hyperpolarized[1-^{13}C]pyruvate. Diabetes. 2016;65:3544.
16. Schroeder M, Laustsen C. Imaging oxygen metabolism with hyperpolarized magnetic resonance: a novel approach for the examination of cardiac and renal function. Biosci Rep. 2017;37.pii: BSR20160186.
17. Laustsen C. Hyperpolarized renal magnetic resonance imaging: potential and pitfalls. Front Physiol. 2016;7:72.
18. Mikkelsen E, Lauridsen H, Nielsen PM, Qi H, Nørlinger T, Andersen MD, Uldbjerg N, Laustsen C, Sandager P, Pedersen M. The chinchilla as a novel animal model of pregnancy. R Soc Open Sci. 2017;4:161098.
19. Markovic S, Fages A, Roussel T, Hadas R, Brandis A, Neeman M, Frydman L. Placental physiology monitored by hyperpolarized dynamic ^{13}C magnetic resonance. Proc Natl Acad Sci U S A. 2018;115:E2429–E2436.
20. Conings S, Amant F, Annaert P, Van Calsteren K. Integration and validation of the ex vivo human placenta perfusion model. J Pharmacol Toxicol Methods. 2017;88:25–31.
21. Mathiesen L, Mose T, Morck TJ, Nielsen JK, Nielsen LK, Maroun LL, Dziegiel MH, Larsen LG, Knudsen LE. Quality assessment of a placental perfusion protocol. Reprod Toxicol. 2010;30:138–146.
22. Gordon Z, Glaubach L, Elad D, Zaretsky U, Jaffa AJ. Ex vivo human placental perfusion model for analysis of fetal circulation in the chorionic plate. J Ultrasound Med. 2016;35:553–560.
23. Friesen-Waldner LJ, Sinclair KJ, Wade TP, Michael B, Chen AP, de Vrijer B, Regnault TR, McKenzie CA. Hyperpolarized [1-(13) C]pyruvate MRI for noninvasive examination of placental metabolism and nutrient transport: a feasibility study in pregnant guinea pigs. J Magn Reson Imaging. 2016;43:750–755.